Observation of angle-modulated switch between enhancement and suppression of nonlinear optical processes

Zhiguo Wang, Zhengyang Zhao, Peiying Li, Jiamin Yuan, Huayan Lan, Huaibin Zheng, Yiqi Zhang, and Yanpeng Zhang[*]

Key Laboratory for Physical Electronics and Devices of the Ministry of Education & Shaanxi Key Lab of Information Photonic Technique, Xi'an Jiaotong University, Xi'an 710049, China
[*]*ypzhang@mail.xjtu.edu.cn*

Abstract: We simultaneously investigate the four-wave mixing and the fluorescence signals via two cascade electromagnetically induced transparency (EIT) systems in atomic rubidium vapor. By manipulating the deflection angle between the probe beam and certain coupling beams, the dark state can extraordinarily switch to bright state, induced by the angle-modulation on the dressing effect. Besides, in the fluorescence signal, the peak of two-photon fluorescence due to classical emission and the dip of single-photon fluorescence due to dressing effect are distinguished, both in separate spectral curves and in the global profile of spectrum. Meanwhile, we observe and analyze the similarities and discrepancies between the two ground-state hyperfine levels $F = 2$ and $F = 3$ of Rb 85 for the first time.

OCIS codes: (190.4380) Nonlinear optics, four-wave mixing; (190.3270) Kerr effect; (190.4180) Multiphoton processes; (300.2570) Four-wave mixing; (270.1670) Coherent optical effects.

References and links

1. C. Li, Y. Zhang, H. Zheng, Z. Wang, H. Chen, S. Sang, R. Zhang, Z. Wu, L. Li, and P. Li, "Controlling cascade dressing interaction of four-wave mixing image," Opt. Express **19**(14), 13675–13685 (2011).
2. N. Li, Z. Zhao, H. Chen, P. Li, Y. Li, Y. Zhao, G. Zhou, S. Jia, and Y. Zhang, "Observation of dressed odd-order multi-wave mixing in five-level atomic medium," Opt. Express **20**(3), 1912–1929 (2012).
3. S. E. Harris, "Electromagnetically induced transparency," Phys. Today **50**(7), 36–42 (1997).
4. M. Xiao, Y. Li, S. Jin, and J. Gea-Banacloche, "Measurement of dispersive properties of electromagnetically induced transparency in rubidium atoms," Phys. Rev. Lett. **74**(5), 666–669 (1995).
5. R. R. Moseley, S. Shepherd, D. J. Fulton, B. D. Sinclair, and M. H. Dunn, "Spatial consequences of electromagnetically induced transparency: observation of electromagnetically induced focusing," Phys. Rev. Lett. **74**(5), 670–673 (1995).
6. S. Wielandy and A. Gaeta, "Investigation of electromagnetically induced transparency in the strong probe regime," Phys. Rev. A **58**(3), 2500–2505 (1998).
7. A. M. Akulshin, S. Barreiro, and A. Lezama, "Electromagnetically induced absorption and transparency due to resonant two-field excitation of quasidegenerate levels in Rb vapor," Phys. Rev. A **57**(4), 2996–3002 (1998).
8. Y. Q. Li and M. Xiao, "Enhancement of nondegenerate four-wave mixing based on electromagnetically induced transparency in rubidium atoms," Opt. Lett. **21**(14), 1064–1066 (1996).
9. Z. Zuo, J. Sun, X. Liu, Q. Jiang, G. Fu, L. A. Wu, and P. Fu, "Generalized n-photon resonant 2n-wave mixing in an (n+1)-level system with phase-conjugate geometry," Phys. Rev. Lett. **97**(19), 193904 (2006).
10. Y. Zhang, A. W. Brown, and M. Xiao, "Opening four-wave mixing and six-wave mixing channels via dual electromagnetically induced transparency windows," Phys. Rev. Lett. **99**(12), 123603 (2007).
11. J. Qi, G. Lazarov, X. Wang, L. Li, L. M. Narducci, A. M. Lyyra, and F. C. Spano, "Autler-Townes splitting in molecular lithium: prospects for all-optical alignment of nonpolar molecules," Phys. Rev. Lett. **83**(2), 288–291 (1999).
12. J. Qi and A. M. Lyyra, "Electromagnetically induced transparency and dark fluorescence in a cascade three-level diatomic lithium system," Phys. Rev. A **73**(4), 043810 (2006).
13. R. W. Boyd, M. S. Malcuit, D. J. Gauthier, and K. Rzaewski, "Competition between amplified spontaneous emission and the four-wave-mixing process," Phys. Rev. A **35**(4), 1648–1658 (1987).
14. C. Li, H. Zheng, Y. Zhang, Z. Nie, J. Song, and M. Xiao, "Observation of enhancement and suppression of four-wave mixing processes," Appl. Phys. Lett. **95**(4), 041103 (2009).

15. Z. Wang, Y. Zhang, H. Zheng, C. Li, F. Wen, and H. Chen, "Switching enhancement and suppression of four-wave mixing via a dressing field," J. Mod. Opt. **58**(9), 802–809 (2011).
16. U. Khadka, Y. Zhang, and M. Xiao, "Control of multitransparency windows via dark-state phase manipulation," Phys. Rev. A **81**(2), 023830 (2010).
17. P. R. S. Carvalho, L. de Araujo, and J. W. R. Tabosa, "Angular dependence of an electromagnetically induced transparency resonance in a Doppler-broadened atomic vapor," Phys. Rev. A **70**(6), 063818 (2004).
18. M. Shuker, O. Firstenberg, R. Pugatch, A. Ben-Kish, A. Ron, and N. Davidson, "Angular dependence of Dicke-narrowed electromagnetically induced transparency resonances," Phys. Rev. A **76**(2), 023813 (2007).
19. Z. Nie, H. Zheng, P. Li, Y. Yang, Y. Zhang, and M. Xiao, "Interacting multiwave mixing in a five-level atomic system," Phys. Rev. A **77**(6), 063829 (2008).
20. U. Khadka, H. Zheng, and M. Xiao, "Four-wave-mixing between the upper excited states in a ladder-type atomic configuration," Opt. Express **20**(6), 6204–6214 (2012).
21. O. Heavens, "Radiative transition probabilities of the lower excited states of the alkali metals," J. Opt. Soc. Am. **51**(10), 1058–1061 (1961).

1. Introduction

The coherent superposition of atomic states forms the base for a great deal of interesting phenomena in nonlinear laser spectroscopy. One of these phenomena resulting from the quantum interference between dressed states [1,2] is electromagnetically induced transparency (EIT) [3–7]. Under EIT condition, several higher-order nonlinear optical processes including four-wave mixing (FWM) [8–10] are allowed to occur in multi-level atomic systems, since the weak generated signals can be allowed to transmit through the resonant atomic medium with little absorption. Meanwhile, the fluorescence due to spontaneous emission can also generate within the EIT windows [11,12] and the competition between amplified spontaneous emission and four-wave-mixing process has been studied [13].

Furthermore, the suppression and enhancement of FWM, which are respectively corresponding to EIT and EIA (electromagnetically induced absorption) of probe transmission, also attracted the attention of many researchers [2,14,15]. By altering the frequency detunings of incident laser fields, the switch between dark state (EIT of probe transmission and suppression of FWM) and bright state (EIA of probe transmission and enhancement of FWM) is obtainable [2,13,15]. It is also reported recently by manipulating the phase difference between the two circularly polarized components of a single coherent field, the EIT-EIA switch could be realized [16].

In this paper, we first report the switch between dark state and bright state by manipulating the deflection angle of certain coupling beams in a Y-type or cascade atomic rubidium system. Such phenomenon is dramatically astonished in comparison with previous works, where only the signal's linewidth changes by altering the angle between beams [17,18]. We have offered a mechanism based on the angle-modulation on the Rabi frequency, which is capable to explain the aforementioned switch. Simultaneously, the FWM signal due to atomic coherence and the fluorescence signals due to spontaneous emission are studied in company with probe transmission signal. By manipulation the deflection angle, the generated FWM and fluorescence processes can also transform from suppression to enhencement along with the EIT-EIA switch in the probe transmission spectrum. Such angle-modulated switch could have potential applications in optical communication and quantum information processing. Moreover, in the fluorescence signal, the peak of two-photon fluorescence due to classical emission and the dip of single-photon fluorescence due to dressing effect are distinguished, both in separate spectral curves and in the global profile of spectrum. Furthermore, the experimental results with two different ground-state hyperfine levels (GSHL) $5S_{1/2}$ $F=2$ and $5S_{1/2}$ $F=3$ of ^{85}Rb are compared for the first time.

2. Basic theory and experimental scheme

2.1 Experimental setup

The experiment is carried out in a rubidium vapor cell, whose energy levels of $5S_{1/2}$ ($|0\rangle$), $5P_{3/2}$ ($|1\rangle$), $5D_{5/2}$ ($|2\rangle$) and $5D_{3/2}$ ($|3\rangle$) form a four-level Y-type atomic system, as shown in Fig. 1(a). The resonant frequencies are Ω_1, Ω_2 and Ω_3 for transitions $|0\rangle$ to $|1\rangle$, $|1\rangle$ to $|2\rangle$ and $|1\rangle$ to $|3\rangle$ respectively. The temperature of the atomic vapor cell is set at 60°C. A weak probe beam E_1 (with frequency ω_1, wave vector $\mathbf{k}_1$, Rabi frequency G_1 and frequency detuning Δ_1, where $\Delta_i = \Omega_i - \omega_i$) from an external cavity diode laser (ECDL), is horizontally polarized and probes the lower transition $|0\rangle$ to $|1\rangle$. Two coupling laser beams E_2 (ω_2, $\mathbf{k}_2$, G_2 and Δ_2) and E_2' (ω_2, $\mathbf{k}_2'$, G_2' and Δ_2) splitting from a cw Ti:sapphire laser with vertical polarization, drive the upper transition $|1\rangle$ to $|2\rangle$. Another two coupling laser beams E_3 (ω_3, $\mathbf{k}_3$, G_3 and Δ_3) and E_3' (ω_3, $\mathbf{k}_3'$, G_3' and Δ_3) splitting from an ECDL with vertical polarization, drive the upper transition $|1\rangle$ to $|3\rangle$. Using this experimental setup, we will study three kinds of signals simultaneously: the transmission of probe beam, the four-wave mixing signals E_{F1} and E_{F2}, and the fluorescence signals R_0, R_1 and R_2 (shown in Fig. 1(a)). Especially, we mainly focus on the control of signal patterns through varying the direction of incident beams.
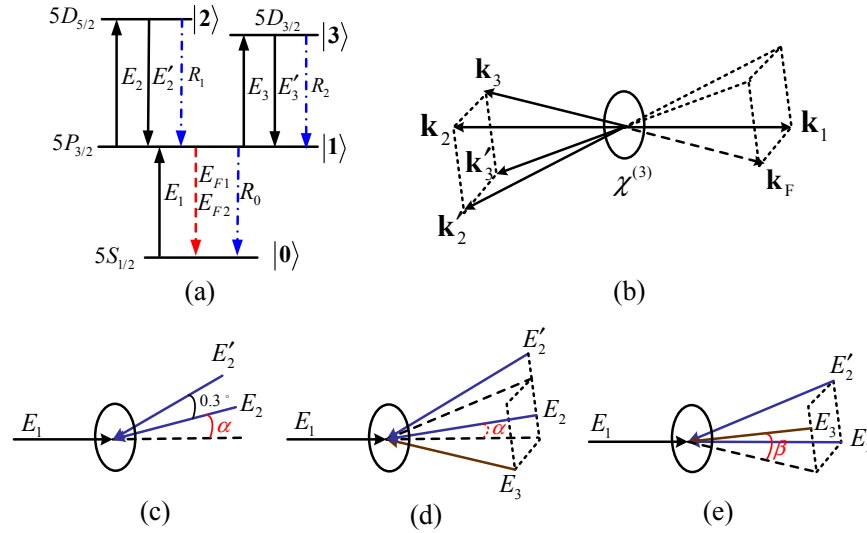
Fig. 1. (a) Relevant four-level Y-type atomic system with one probe field E_1, two coupling fields E_2 and E_2', and another two coupling fields E_3 and E_3'. E_{F1} and E_{F2} are the generated FWM signals. R_0, R_1 and R_2 are the generated fluorescence signals. (b) Normal phase-matching spatial beam geometry. (c)-(e) The abnormal propagation configurations for the ladder type subsystem and Y-type system, with the deflection angles α and β. The dash lines in (c)-(e) represent the direction of beams when the deflection angles equal 0°.

In normal experimental configuration, the five laser beams are spatially designed in a square-box pattern as shown in Fig. 1(b), in which the coupling beams E_2, E_2', E_3 and E_3'

propagate through the Rb vapor cell in the same direction with small angles (about $0.3°$) between one another, and the probe beam E_1 propagates in the opposite direction of E_2. In such beam geometric configuration, the two-photon Doppler-free conditions will be satisfied for the two ladder-type subsystems $|0\rangle - |1\rangle - |2\rangle$ and $|0\rangle - |1\rangle - |3\rangle$, thus two EIT windows appear in the probe transmission spectrum. Also, two FWM processes E_{F1} (generated by E_1, E_2 and E_2') and E_{F2} (generated by E_1, E_3 and E_3') can occur simultaneously within the two EIT windows, both propagating in the direction of $\mathbf{k}_F$ (at the lower right corner of Fig. 1(b)) satisfying the phase-matching condition $\mathbf{k}_{F1} = \mathbf{k}_1 + \mathbf{k}_2 - \mathbf{k}_2'$ or $\mathbf{k}_{F2} = \mathbf{k}_1 - \mathbf{k}_3' + \mathbf{k}_3$. In our experiments, we used a silicon photodiode to monitor the transmitted probe spectrum, and an avalanche photodiode detector to measure the generated FWM signals.

In addition to FWM signals induced by atomic coherence, three fluorescence signals due to spontaneous emission are studied simultaneously: the decay of photons from $|1\rangle$ to $|0\rangle$ generate single-photon fluorescence signal R_0, and the decay of photons from $|2\rangle$ or $|3\rangle$ to $|1\rangle$ separately generate two-photon fluorescence signals R_1 and R_2, as shown in Fig. 1(a). These non-directional fluorescence signals are collected by a photodiode located at the side of the vapor cell. Similar to FWM signals, the two-photon fluorescence R_1 and R_2 also fall into the EIT windows and form the Doppler-free sharp peaks in frequency domain.

In our experiments, we especially focus on the angle-modulated switch on the probe transmission signal, FWM signals and fluorescence signals. When certain coupling beams are deflected with a small angle from their "normal" directions, the behaviors of the detected signals will change significantly: EIT peak in the probe transmission spectrum would switch to EIA dip; the suppression of FWM signal would alter to enhancement; and the pattern of fluorescence signals would also change correspondingly. We use the symbol α to represent the deflection of the coupling beams E_2 and E_2' from their normal directions (as shown in Fig. 1(c)-1(d)), and use the symbol β to represent the deflection of the coupling beams E_3 and E_3' from their normal directions (as shown in Fig. 1(e)). By altering the deflection angle α or β in different conditions, we can observe the switches of signals' pattern we stated above. In the following we term such deflected spatial geometry (Fig. 1(c)-1(e)) the "abnormal" propagation configuration, to distinguish it from the "normal" spatial geometry shown in Fig. 1(b).

2.2 Basic theory

Generally, the behaviors of detected signals can be described by density matrix elements with different orders. Specially, the probe transmission signal can be described by the opposite of the imaginary part of first-order density matrix element $\rho_{10}^{(1)}$ (the superscript of the notation represents the order of density matrix element, or perturbation order), the intensity of FWM signals can be described by the third-order one $\rho_{10}^{(3)}$, and the intensity of fluorescence signals are related to the even-order ones $\rho_{11}^{(2)}$, $\rho_{22}^{(4)}$ and $\rho_{33}^{(4)}$, which are the various diagonal elements of the density matrix. The expressions of these elements can be obtained by solving the coupled density-matrix equations [12,19].

Via the Liouville pathway (perturbation chain) $\rho_{00}^{(0)} \xrightarrow{E_1} \rho_{10}^{(1)}$, the element $\rho_{10}^{(1)}$ can be written as:

$$\rho_{10}^{(1)} = iG_1 / d_1, \tag{1a}$$

with $d_1 = \Gamma_{10} + i\Delta_1$ (Γ_{ij} is the transverse relaxation rate between $|i\rangle$ and $|j\rangle$). The opposite of the imaginary part of $\rho_{10}^{(1)}$ is proportional to the transparency degree of probe beam. When further considering the strong dressing effect of coupling fields $E_2(E_2')$ and $E_3(E_3')$, the energy level $|1\rangle$ was split to two dressed states $|+\rangle$ and $|-\rangle$, thereby $\rho_{10}^{(1)}$ is revised as:

$$\rho_{10SD}^{(1)} = iG_1 / (d_1 + |G_2|^2 / d_2), \qquad (1b)$$

$$\rho_{10DD}^{(1)} = iG_1 / (d_1 + |G_2|^2 / d_2 + |G_3|^2 / d_3), \qquad (1c)$$

with $d_2 = \Gamma_{20} + i(\Delta_1 + \Delta_2)$ and $d_3 = \Gamma_{30} + i(\Delta_1 + \Delta_3)$, (the subscript SD means single-dressed, DD means double-dressed). Via the pathway $\rho_{00}^{(0)} \xrightarrow{E_1} \rho_{10}^{(1)} \xrightarrow{E_2} \rho_{20}^{(2)} \xrightarrow{(E_2')^*} \rho_{10}^{(3)}$, the FWM process E_{F1} can be described by:

$$\rho_{F1DD}^{(3)} = -iG_1 G_2 (G_2')^* / [(d_1 + |G_2|^2 / d_2 + |G_3|^2 / d_3)^2 d_2] \qquad (2)$$

with doubly dressing effect. Similarly, the FWM process E_{F2} can be described by:

$$\rho_{F2DD}^{(3)} = -iG_1 G_3 (G_3')^* / [(d_1 + |G_2|^2 / d_2 + |G_3|^2 / d_3)^2 d_3] \qquad (3)$$

with doubly dressing effect.

For the fluorescence signals, the intensity of single-photon fluorescence (R_0) and two-photon fluorescence (R_1 and R_2) are separately proportional to the square of the module of second-order matrix element ($\rho_{11}^{(2)}$) and fourth-order matrix elements ($\rho_{22}^{(4)}$ and $\rho_{33}^{(4)}$), since the square of the module of diagonal elements represent the density of particles in corresponding states. First of all, with only probe beam E_1 turned on, the single-photon fluorescence signal R_0 generates, the process of which is described by the pathway $\rho_{00}^{(0)} \xrightarrow{E_1} \rho_{10}^{(1)} \xrightarrow{(E_1)^*} \rho_{11}^{(2)}$. Guided by the pathway, we can easily obtain the expression of $\rho_{11}^{(2)}$ from the density-matrix equations, as:

$$\rho_{11}^{(2)} = -|G_1|^2 / (\Gamma_{11} d_1). \qquad (4a)$$

With $E_2(E_2')$ and $E_3(E_3')$ also turned on, R_0 can get singly or doubly dressed:

$$\rho_{11SD}^{(2)} = -|G_1|^2 / [\Gamma_{11}(d_1 + |G_2|^2 / d_2)], \qquad (4b)$$

$$\rho_{11DD}^{(2)} = -|G_1|^2 / [\Gamma_{11}(d_1 + |G_2|^2 / d_2 + |G_3|^2 / d_3)]. \qquad (4c)$$

Especially, if we further simplify Eqs. (1a)-(1c) and Eqs. (4a)-(4c), we discover the square of the module of $\rho_{11}^{(2)}$ and the imaginary part of $\rho_{10}^{(1)}$ behave similarly. Therefore we assume the single-photon fluorescence signal and the probe transmission signal behave in corresponding manners. This hypothesis would be verified by both experimental results and simulations in the following sections.

Next, in the two ladder type subsystems $|0\rangle - |1\rangle - |2\rangle$ and $|0\rangle - |1\rangle - |3\rangle$, the two-photon fluorescence signals R_1 and R_2 generate separately. In $|0\rangle - |1\rangle - |2\rangle$ subsystem, the generation of R_1 can be described by $\rho_{00}^{(0)} \xrightarrow{E_1} \rho_{10}^{(1)} \xrightarrow{E_2} \rho_{20}^{(2)} \xrightarrow{(E_1)^*} \rho_{21}^{(3)} \xrightarrow{(E_2)^*} \rho_{22}^{(4)}$.

Step by step guided by the pathway, we can get the expressions of related elements: $\rho_{10}^{(1)} = -iG_1/d_1$ via $\rho_{00}^{(0)} \xrightarrow{E_1} \rho_{10}^{(1)}$, $\rho_{20}^{(2)} = -G_1G_2/(d_1d_2)$ via $\rho_{10}^{(1)} \xrightarrow{E_2} \rho_{20}^{(2)}$, $\rho_{21}^{(3)} = iG_1^2G_2/(d_1d_2d_4)$ ($d_4 = \Gamma_{21} + i\Delta_2$) via $\rho_{20}^{(2)} \xrightarrow{(E_1)^*} \rho_{21}^{(3)}$, and finally:

$$\rho_{22}^{(4)} = G_1^2 G_2^2/(\Gamma_{22}d_1d_2d_4) \tag{5a}$$

via $\rho_{21}^{(3)} \xrightarrow{(E_2)^*} \rho_{22}^{(4)}$. Considering the dressing effect of $E_2(E_2')$, $\rho_{22}^{(4)}$ is modified into:

$$\rho_{22SD}^{(4)} = |G_1|^2 |G_2|^2/[\Gamma_{22}d_1d_4(d_2 + |G_2|^2/d_1)]. \tag{5b}$$

Similarly, in the $|0\rangle - |1\rangle - |3\rangle$ subsystem the element $\rho_{33}^{(4)}$ related to the other two-photon fluorescence signal R_2 can be written as:

$$\rho_{33}^{(4)} = |G_1|^2 |G_3|^2/(\Gamma_{33}d_1d_5d_3), \tag{6a}$$

with $d_5 = \Gamma_{31} + i\Delta_3$ via the pathway $\rho_{00}^{(0)} \xrightarrow{E_1} \rho_{10}^{(1)} \xrightarrow{E_3} \rho_{30}^{(2)} \xrightarrow{(E_1)^*} \rho_{31}^{(3)} \xrightarrow{(E_3)^*} \rho_{33}^{(4)}$. Considering the dressing effect of $E_3(E_3')$, $\rho_{33}^{(4)}$ is modified into:

$$\rho_{33SD}^{(4)} = |G_1|^2 |G_3|^2/[\Gamma_{33}d_1d_5(d_3 + |G_3|^2/d_1)] \tag{6b}$$

When the coupling beams are deflected with a small angle α or β, because of phase matching conditions, the coupling strength (Rabi frequency) becomes a function of the angles. As is known, Rabi frequency G_i is defined as $G_i = \mu_i E_i \cos\theta/\hbar$ where E_i represents the electric field, μ_i is the dipole moment of transition the light field excites, and θ represents the angle between the polarization of the light and the transition dipole moment. Now, when the additional deflection angle α between E_2 and the opposite direction of E_1 is introduced in, the orientation of electric field E_2 changes, and the Rabi frequency G_2 should be modified as $G_2 = \mu_2 E_2 \cos(\theta \pm \alpha)/\hbar$. Similarly, when the beam E_3 is deflected with the angle β, the Rabi frequency G_3 should be modified as $G_3 = \mu_3 E_3 \cos(\theta \pm \beta)/\hbar$. In a word, by manipulating the deflection angles, we can control the coupling strength, and thereby control the switch between dark state and bright state. Although the angles α or β are relatively small, we will find the signals are strikingly sensitive to their alterations.

3. Observation of angle modulation in ladder type subsystem

We have deduced the expressions of related density matrix elements and discussed the mechanism of angle-modulated switch. In the following sections, we will present the experimental results of angle modulation in ladder type subsystem (this section), in Y-type system (Sec. 4), and the direct observation of angle-modulated suppression-enhancement switch of FWM (Sec. 5).

We first consider the angle modulation in the $|0\rangle - |1\rangle - |2\rangle$ ladder type subsystem when three beams E_1, E_2 and E_2' are turned on (as shown in Fig. 1(c)). We separately show the results with the two ground-state hyperfine levels (GSHL) of ^{85}Rb: $5S_{1/2}$ $F=3$ in Fig. 2 and $5S_{1/2}$ $F=2$ in Fig. 3. In both cases the angle modulation effect can be observed clearly, but some discrepancies can also be observed in the results with two different ground states.

In Figs. 2(a)-2(c), the probe transmission (Figs. 2(a1)-2(a4)), FWM (Figs. 2(b1)-2(b4)) and fluorescence signals (Figs. 2(c1)-2(c4)) are presented simultaneously, obtained by scanning Δ_2 with probe detuning Δ_1 and deflection angle α separately set at typical values. The

obtained signals are arranged in a three-dimensional box, so that the variation of the curves versus both Δ_1 and α is explicitly displayed. When the beams E_2 and E_2' propagate from their normal direction without deflection ($\alpha = 0\,°$), in the probe transmission spectrum we can see EIT (peaks higher than the baseline) appearing in the center area within the Doppler absorption background, EIA (small dips lower than the base lines) emerging at large probe detunings, and partial-EIT-partial-EIA appearing in the transitional areas (as shown in Fig. 2(a2)), this is just the same as the results in previous work [2]. However, when the coupling beams are deflected from normal directions ($\alpha \neq 0\,°$, as the geometry shown in Fig. 1(c)), switches between EIA and EIT can be observed at each Δ_1 point. For example, in the case of $\alpha = -0.08\,°$ (Fig. 2(a1)), strong EIT peak appears at negative Δ_1 points, and EIA dip appears at positive Δ_1 points. On the contrary, when α is set at positive values (Figs. 2(a3)-2(a4)), obvious EIA dip appears at negative Δ_1 points, while EIT peak emerges at positive probe detunings. In sum, when $\alpha \neq 0\,°$, the symmetrical pattern of probe transmission versus Δ_1 is broken. We also present the simulation of such EIT-EIA switch, as shown in Figs. 2(d1)-2(d3), which is in agreement with the experimental results.
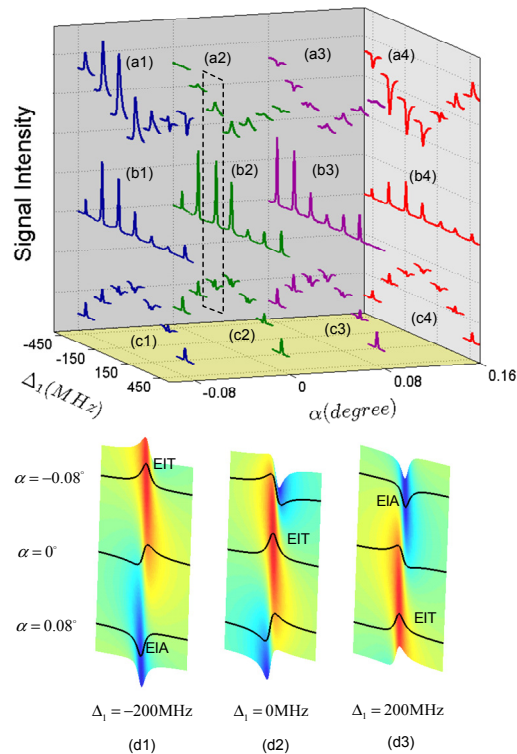
Fig. 2. (a)-(c) Measured signals versus Δ_2 at discrete probe detuning Δ_1 and discrete deflection angle α, the ground-state is $5S_{1/2}$ $F=3$. The top curves ((a1)-(a4)) are probe transmission; the middle curves ((b1)-(b4)) are FWM signal; and the bottom curves ((c1)-(c4)) are fluorescence signal. The experimental parameters are $P_1 = 8\text{mW}$, $P_2 = 10\text{mW}$ and $P_2' = 10\text{mW}$. (d1)-(d3) Calculated probe transmission versus α at three typical detunings.

As is known, the suppression of FWM is obtained in EIT window, and the enhancement of FWM is in company with EIA. Thus the switch between the suppression and enhancement of FWM will appear along with the EIT-EIA switch. In Figs. 2(b1)-2(b4), the suppression-enhancement switch of FWM is reflected in the variation in signal's intensity with different angles. For instance, when α is set at $-0.08°$ (Fig. 2(b1)) or $0°$ (Fig. 2(b2)), the FWM signal reaches its maximum at $\Delta_1 = -300\text{MHz}$; and when α is set at $0.08°$ (Fig. 2(b3)), it reaches the maximum around $\Delta_1 = -450\text{MHz}$. Admittedly, there're some other factors which could also lead to the variation in the intensity of FWM. For instance, the FWM generally weakens with α increasing, because the effective overlap cross section of the beams generating FWM decreases. Therefore analyzing the variation in the intensity of FWM is not an ideal way to observe the suppression-enhancement switch. In Sec. 5, we will observe the switch in FWM directly using another method.
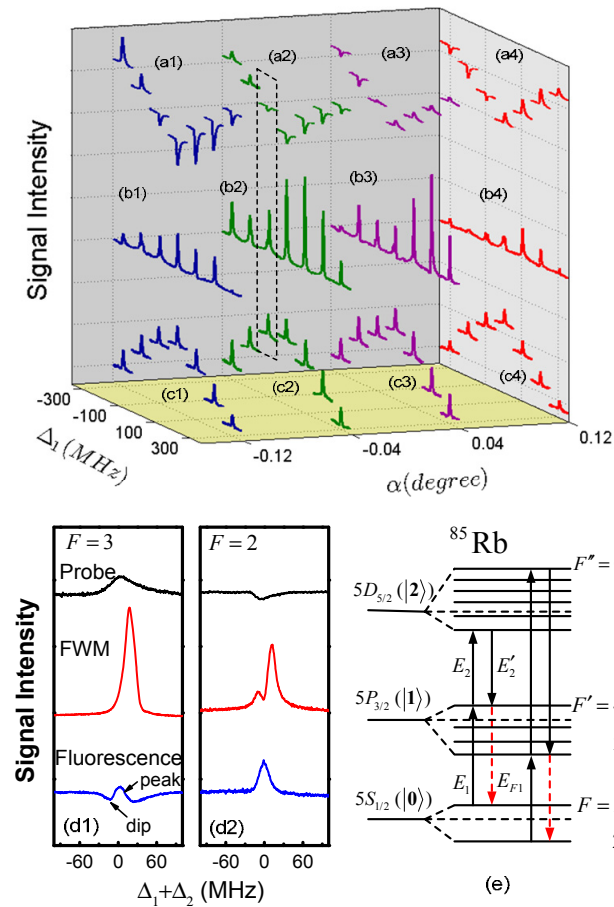
Fig. 3. (a)-(c) Measured signals versus Δ_2 at discrete Δ_1 and α, the ground state is $5S_{1/2}$ $F=2$. The experimental parameters are the same as Fig. 2. (d1)-(d2) Magnified sub-graphs for $5S_{1/2}$ $F=3$ and $F=2$ of ^{85}Rb. (e) Realistic energy level diagram showing the hyperfine levels of each driven state, where the FWM transitions with the least number of decay channels are presented.

The fluorescence signals (Figs. 2(c1)-2(c4)) is composed of two components: the single-photon fluorescence R_0 related to matrix element $\rho_{11}^{(2)}$ and the two-photon fluorescence R_1 related to matrix element $\rho_{22}^{(4)}$. Basically, the obtained fluorescence signal appears as a dip containing a sharp peak on each base line (details can be clearly seen in the amplified sub-figure in Fig. 3(d1)). The dip represents the suppression of R_0 induced by the dressing effect of E_2 (E_2'), corresponding with EIT in probe transmission spectrum. The peak within the dip is the emission of fluorescence R_1, which is corresponding with EIA according to Eqs. (1b) and (5b). Therefore, in the process of altering the angle α, R_0 will get stronger suppression when EIT appears, and R_1 will be enhanced in the presence of EIA (more clear details will be shown in Fig. 4).

Now we turn to the results for the other ground state: $5S_{1/2}$ $F=2$ of ^{85}Rb (Figs. 3(a)-3(c)). The phenomenon of angle-modulation for $F=2$ is similar with $F=3$, except for some discrepancies. To show the details clearly, we magnified two typical sub-graphs from Figs. 2(a)-(c) and Figs. 3(a)-3(c) respectively, as shown in Figs. 3(d1)-3(d2). In the case of $F=3$ (Fig. 2(a)), when Δ_1 is set at negative points (for example $\Delta_1 = -300$MHz), the probe transmission signal can change from strong EIT ($\alpha = -0.08°$), to weak EIT ($\alpha = 0°$), then to weak EIA ($\alpha = 0.08°$), and finally to strong EIA ($\alpha = 0.16°$). But when Δ_1 is set at positive points, the switch process is not as striking as above. By contrast, in the case of $F=2$ (Fig. 3(a)), the striking EIA-EIT switch happens in positive probe detuning region. Besides, the strongest FWM generation also appears in positive probe detuning region for $F=2$ (Fig. 3(b)), which is different from the case of $F=3$ where the strongest FWM appears in negative detuning region (Fig. 2(b)). Moreover, the fluorescence signals for the two ground states are also different. Comparing the fluorescence signal for $F=2$ with that for $F=3$, we find the suppression dip of fluorescence disappears for $F=2$ ground state (Fig. 3(d2)). These discrepancies could be explained with the assistance of the realistic energy level diagram in Fig. 3(e). For the ground state $F=3$, the higher frequency transition $F=3 \rightarrow F'=4$ is closed; in other words the pathways involving $F'=4$ have the fewest decay channels. Therefore the FWM generation and the switch for $F=3$ are strongest in the negative-detuned region where the $F'=4$ level lies [20]. On the contrary, for the ground state $F=2$, the lower frequency transition $F=2 \rightarrow F'=1$ is closed. That's why for $F=2$ the strongest FWM and switch appear in positive-detuned region.

In following sections, the experiments are all performed with ground state $F=3$ of ^{85}Rb.

4. Observation of angle modulation in Y-type subsystem

In this section, we emphasize on the angle modulation in the Y-type system where the doubly dressing effect should be considered. First in Fig. 4, with E_1, E_2, E_2' and E_3 turned on and E_3' blocked (as the geometry shown in Fig. 1(d)), we study the signals by scanning Δ_2 at different Δ_3 points, with the angle α set at two typical values $\alpha = 0.04°$ (Fig. 4(a)) and $\alpha = 0.16°$ (Fig. 4(c)). The theoretical calculations corresponding to Figs. 4(a) and 4(c) are presented in Figs. 4(b) and (d).

Under the doubly dressing condition, two EIT would form simultaneously in the probe transmission spectrum: the $|0\rangle - |1\rangle - |2\rangle$ EIT and the $|0\rangle - |1\rangle - |3\rangle$ EIT. In the case of $\alpha = 0.04°$, the global profile of the transmitted probe signal (Fig. 4(a1)) versus Δ_3 reaches its summit at $\Delta_3 = -\Delta_1 = 0$, representing the $|0\rangle - |1\rangle - |3\rangle$ EIT window; on the other hand,

the peak on each curve versus Δ_2 is the $|0\rangle-|1\rangle-|2\rangle$ EIT window, satisfying $\Delta_1+\Delta_2=0$. When α is adjusted to $\alpha=0.16\,^\circ$, the $|0\rangle-|1\rangle-|2\rangle$ EIT peaks can be observed totally switch to EIA dips, as shown in Fig. 4(c1). Notice the $|0\rangle-|1\rangle-|3\rangle$ EIT profile remains the same under the two angles, because changing the direction of E_2 and E_2' will not influence the dressing effect of E_3.
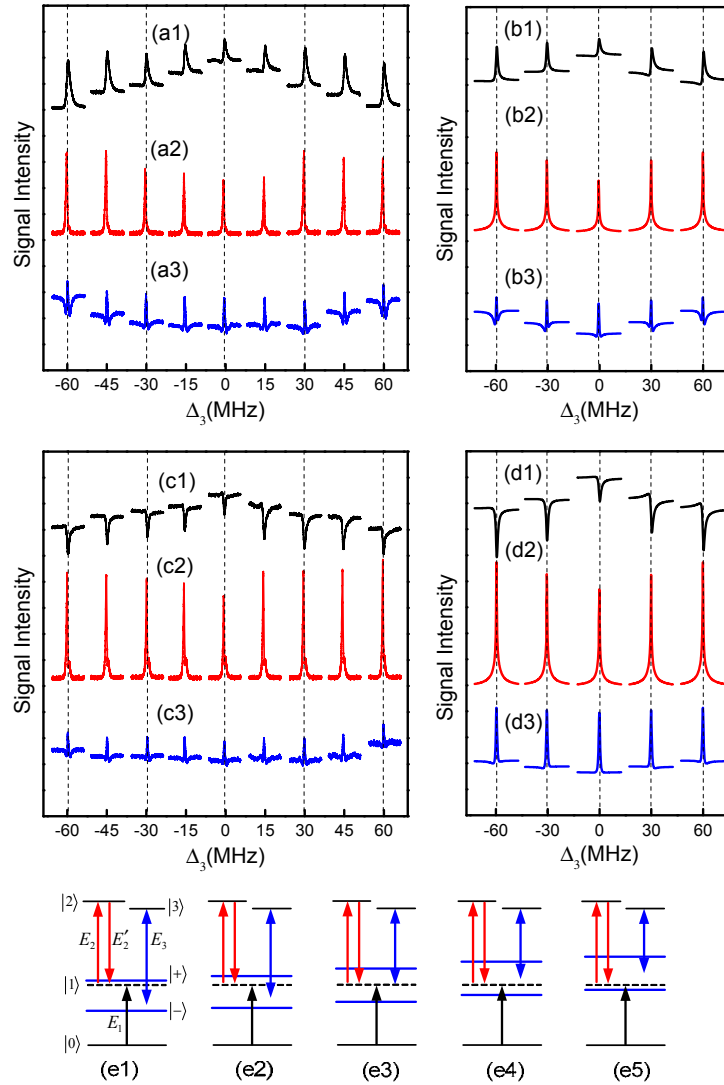
Fig. 4. (a) and (c) Measured probe transmission (top curves), FWM signal E_{F1} (middle curves), and fluorescence signal (bottom curves) versus Δ_2 at discrete Δ_3, with fixed $\Delta_1=0$MHz and E_3' blocked. For (a1)-(a3) $\alpha=0.04\,^\circ$, and for (c1)-(c3) $\alpha=0.16\,^\circ$. The other parameters are $P_1=7.8$mW, $P_2=6.9$mW, $P_2'=15.9$mW and $P_3=46.0$mW. (b) and (d) The calculated curves corresponding to (a) and (c) respectively. (e) The corresponding dressed state diagrams with typical Δ_3 values.

In Fig. 4(a1) and 4(c1), when comparing the curves at $\Delta_3 = 0\text{MHz}$, $\Delta_3 = \pm 30\text{MHz}$ and $\Delta_3 = \pm 60\text{MHz}$, one can discover that both the $|0\rangle - |1\rangle - |2\rangle$ EIT in Fig. 4(a1) and the $|0\rangle - |1\rangle - |2\rangle$ EIA in Fig. 4(c1) reach their minimum amplitude at $\Delta_3 = 0\text{MHz}$, matching the condition $\Delta_1 + \Delta_2 = \Delta_1 + \Delta_3 = 0$. This is due to the strong sequential-cascade-dressing interaction between the two ladder type subsystems $|0\rangle - |1\rangle - |2\rangle$ and $|0\rangle - |1\rangle - |3\rangle$, according to the doubly dressed term $d_1 + |G_2|^2 / d_2 + |G_3|^2 / d_3$ in Eq. (1c). Such interaction can be illustrated with the dressed state diagrams in Fig. 4(e). Figures 4(e1)-4(e5) separately present the diagrams of dressed states with Δ_3 gradually altering from negative to positive. Due to the dressing effect of E_3, the energy level $|1\rangle$ would be split into two dressed states $|+\rangle$ and $|-\rangle$, the positions of which altering along with Δ_3. As we know, the larger the relative frequency of a field to the transition it drives, the weaker the dressing effect is. When $\Delta_3 = 0\text{MHz}$ (Fig. 4(e3)), the relative frequency of E_2 (E_2') to the transition $|+\rangle \rightarrow |2\rangle$ or $|-\rangle \rightarrow |2\rangle$ is large, therefore the dressing effect of E_2 (E_2') is relatively weak and the $|0\rangle - |1\rangle - |2\rangle$ EIT/EIA is small; with $|\Delta_3|$ increasing, the relative frequency of E_2 (E_2') to one of the two transitions $|+\rangle \rightarrow |2\rangle$ and $|-\rangle \rightarrow |2\rangle$ gets smaller, therefore the dressing effect of E_2 (E_2') becomes larger and the $|0\rangle - |1\rangle - |2\rangle$ EIT/EIA becomes stronger.

For the FWM signal E_{F1} generated by E_1, E_2 and E_2' shown in Fig. 4(a2), we can see its intensity is much weaker at resonant point ($\Delta_3 \approx -\Delta_1 = 0$) than at detuned Δ_3, for the suppression of the external dressing field E_3 on E_{F1} is strongest around $\Delta_3 = -\Delta_1$. When α is adjusted to $0.16°$ (Fig. 4(c2)), E_{F1} is greatly strengthened at each Δ_3 point. This is for the reason that the original suppression effect on E_{F1} induced by the self-dressing fields E_2 (E_2') transforms to enhancement effect when $\alpha = 0.16°$, corresponding to the switch from EIT to EIA of the transmitted probe field.

The fluorescence signal in Figs. 4(a3) and 4(c3) includes the doubly dressed single-photon fluorescence R_0, and the two-photon fluorescence R_1. For R_0, on the one hand it is suppressed by E_3 to its minimum around $\Delta_3 \approx -\Delta_1 = 0$, corresponding to the $|0\rangle - |1\rangle - |3\rangle$ EIT profile in Figs. 4(a1) and (c1); on the other hand it is also suppressed by E_2 (E_2'), shown as the dip on each curve, corresponding to the $|0\rangle - |1\rangle - |2\rangle$ EIT peak. The sharp peak within each dip represents the emission of the two-photon fluorescence R_1. It is obvious in Fig. 4(a3) that the suppression dip of R_0 induced by E_2 (E_2') gets much shallower when Δ_3 approaches the resonant point, in agreement with the weakened $|0\rangle - |1\rangle - |2\rangle$ EIT peaks around $\Delta_3 = 0$ in Fig. 4(a1). Under the condition of $\alpha = 0.16°$ (Fig. 4(c3)), the suppression dip on each curve become shallower compared with those in Fig. 4(a3). This corresponds to the behavior of probe transmission signal which changes from EIT ($\alpha = 0.04°$) to EIA ($\alpha = 0.16°$). To make the facts above more evident, we present the corresponding theoretical calculated results in Figs. 4(b) and 4(d), which are in good agreement with the experimental results in Figs. 4(a) and 4(c).

Next, the generated signals under a specific abnormal configuration ($\alpha = 0.16°$) are present in Fig. 5, where we will put emphasis on the variation of fluorescence signals in particular. Figures 5(a) and (c) present the measured signals by scanning Δ_2 at different Δ_3

points with $\alpha = 0.16$ °, in which the probe detuning Δ_1 is set at $\Delta_1 = 0$MHz for Fig. 5(a) and $\Delta_1 = -150$MHz for Fig. 5(c). Similar with the case in Fig. 4(c1), the abnormal EIA dip instead of normal EIT peak appears around $\Delta_1 + \Delta_3 = 0$ in the transmitted probe spectrum, due to the modulation of angle α. However, we notice the EIA dip in Figs. 5(a1) and 5(c1) emerges only in a small region around $\Delta_1 + \Delta_3 = 0$, whereas the EIA in Fig. 4(c1) appears in a extensive region, this is the result of the smaller probe field power P_1 in Fig. 5 compared with Fig. 4. For the FWM signal in Figs. 5(a2) and 5(c2), it's obvious that the intensity is greatly larger at the detuning point $\Delta_1 = -150$MHz (Fig. 5(c2)) than at $\Delta_1 = 0$MHz (Fig. 5(a2)), due to the different numbers of decay channels between transitions, which has already been discussed in Sec. 3.
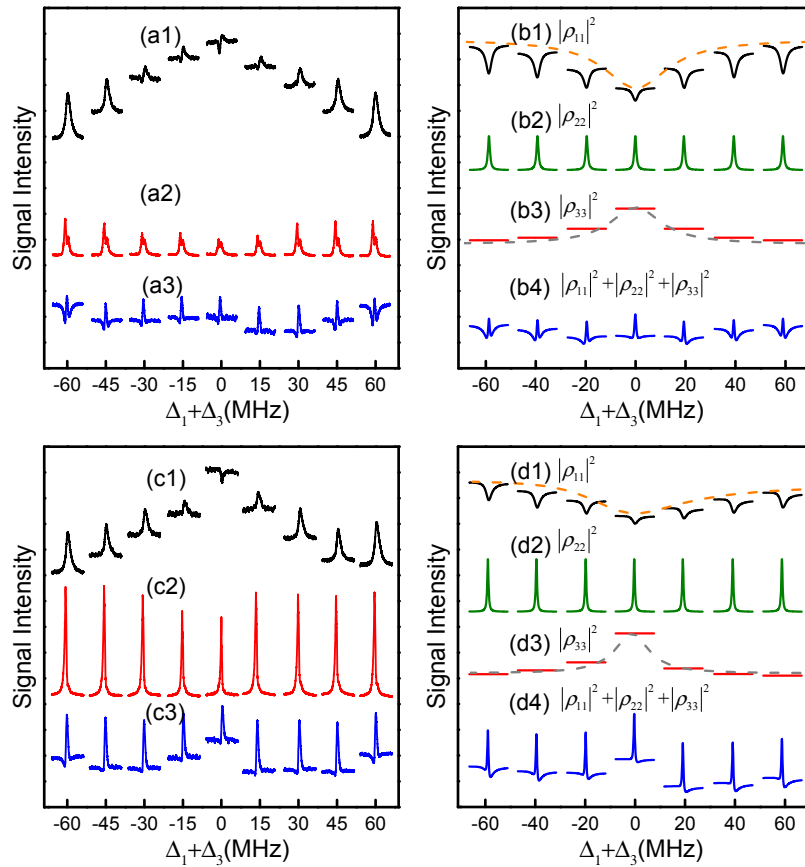
Fig. 5. (a) and (c) Measured probe transmission (top curves), FWM signal E_{F1} (middle curves), and fluorescence signals (bottom curves) versus Δ_2 at discrete Δ_3, with $\alpha = 0.16$ °, E_3' blocked and Δ_1 fixed at $\Delta_1 = 0$MHz for (a) and $\Delta_1 = -150$MHz for (c). The other parameters are $P_1 = 4$mW, $P_2 = 12.6$mW, $P_2' = 6.3$mW and $P_3 = 40$mW. (b) and (d) Calculated fluorescence signals corresponding to (a3) and (c3) separately.

When we turn to the fluorescence signals in Figs. 5(a3) and 5(c3), we find all three types of fluorescence (R_0, R_1 and R_2) arise in the spectrum under such experimental condition. To discriminate them clearly, we present the corresponding calculated fluorescence signals as R_0 ($\sim|\rho_{11}|^2$), R_1 ($\sim|\rho_{22}|^2$), R_2 ($\sim|\rho_{33}|^2$) and the total fluorescence signal ($\sim|\rho_{11}|^2+|\rho_{22}|^2+|\rho_{33}|^2$) separately in Figs. 5(b) and 5(d), among which the calculated total fluorescence signal in Figs. 5(b4) and 5(d4) is the simulation of the experimental detected fluorescence signal in Figs. 5(a3) and 5(c3). When $\Delta_1=0$MHz, the calculated single-photon fluorescence R_0 is shown in Fig. 5(b1), where we can see each curve reveals as a dip resulting from the suppression effect of E_2 (E_2'). Besides, the global profile of the curves also reveals as a big dip (shown as the dash line), for R_0 is also suppressed by E_3. Figs. 5(b2) and 5(b3) show the two-photon fluorescence R_1 and R_2, respectively. Under the method of scanning Δ_2 at different Δ_3 points, the fluorescence signal R_1 reveals as an emission peak on each spectral line (Fig. 5(b2)); while the fluorescence signal R_2 reveals as an emission profile composed of a series of horizontal lines at each Δ_3 point (Fig. 5(b3)). Therefore, when we turn to the total fluorescence signal in Fig. 5(b4), it is obvious that its intensity versus Δ_2 (the curve at each Δ_3 point) reveals as a dip (the suppression induced by E_2 (E_2') on R_0) containing a sharp peak (R_1), and fluorescence intensity versus Δ_3 (the global profile of curves at different Δ_3 points) also behaves as a dip (the suppression induced by E_3 on R_0) containing a peak (R_2).

When Δ_1 is tuned away from resonance, the amplitudes of both the suppression dips and the emission peaks change, as shown in Fig. 5(d). First, the suppression dips of R_0 both in the profile and in each curve become shallower in Fig. 5(d1) compared with those in Fig. 5(b1), since the dressing effect weakens with detuned probe field. On the other hand, both R_1 peak (Fig. 5(d2)) and R_2 peak (Fig. 5(d3)) get stronger, compared with those in Figs. 5(b2) and (b3). According to Eqs. (5b) and (6b), the two-photon fluorescence signals are under suppression around $\Delta_1=0$MHz, and such suppression effects weaken when $|\Delta_1|$ increases. This is why R_1 and R_2 get strong with detuned Δ_1.

Next, with all the five beams turned on, we investigate the function of deflection angle α in the interplay of two ladder type subsystems $|0\rangle-|1\rangle-|2\rangle$ and $|0\rangle-|1\rangle-|3\rangle$, as shown in Fig. 6. Here, the probe detuning Δ_1 is scanned with Δ_2 set at four different values, and we present the experimental results with two different angles: $\alpha=0°$ for Figs. 6(a1)-6(a4); and $\alpha=0.12°$ for Figs. 6(b1)-6(b4).
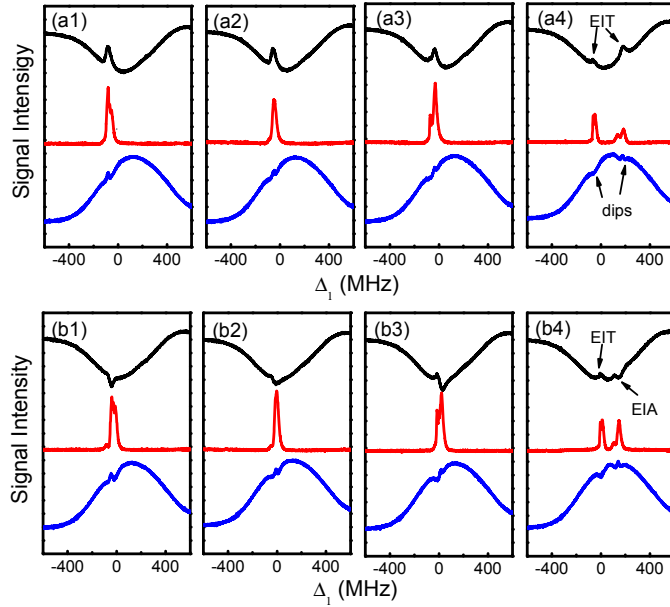
Fig. 6. Measured probe transmission (top curves), FWM (middle curves) and fluorescence (bottom curves) versus Δ_1 when all the beams are turned on. The coupling detuning Δ_2 is set at 80MHz ((a1) and (b1)), 60MHz ((a2) and (b2)), 40MHz ((a3) and (b3)), and -150MHz ((a4) and (b4)); Δ_3 is fixed at $\Delta_3=60\text{MHz}$. α is set at $\alpha=0°$ for (a1)-(a4), and $\alpha=0.12°$ for (b1)-(b4). The other experimental parameters are $P_1=8.2\text{mW}$, $P_2=18.3\text{mW}$, $P_2'=9.6\text{mW}$, $P_3=29.0\text{mW}$, and $P_3'=25.0\text{mW}$.

In the former case (Figs. 6(a1)-6(a4)), two EIT windows separately related to the ladder-type subsystems $|0\rangle-|1\rangle-|2\rangle$ and $|0\rangle-|1\rangle-|3\rangle$ appear in the probe transmission spectrum (the top curves). Simultaneously, two FWM signals E_{F1} and E_{F2} (the middle curves) are generated within the two EIT windows. In the fluorescence signals (the bottom curves), the background curve revealing the emission profile of single-photon fluorescence R_0, two dips appear at $\Delta_1=-\Delta_2$ and $\Delta_1=-\Delta_3$ upon the emission profile representing the suppression induced by $E_2(E_2')$ and $E_3(E_3')$, respectively. Here by scanning Δ_1, the hypothesis that R_0 could be regard as the counterpart of the probe transmission signal is reconfirmed: the emission profile of R_0 is corresponding to the absorption background of the probe transmission spectrum, and the two suppression dips of R_0 are corresponding to the two EIT windows. Besides, within the two suppression dips of R_0 the two-photon fluorescence signals R_1 and R_2 are generated as small peaks, respectively (although R_2 signal at $\Delta_1=-\Delta_3$ is unobvious).

As Δ_3 is fixed at 60MHz and Δ_2 is changed from 80MHz (Fig. 6(a1)), to 60MHz (Fig. 6(a2)), 40MHz (Fig. 6(a3)) and finally to -150MHz (Fig. 6(a4)), the measured signals related to $|0\rangle-|1\rangle-|3\rangle$ subsystem ($|0\rangle-|1\rangle-|3\rangle$ EIT, E_{F2} and R_2) are always fixed at $\Delta_1=-\Delta_3=-60\text{MHz}$, and the characteristic signals related to $|0\rangle-|1\rangle-|2\rangle$ subsystem ($|0\rangle-|1\rangle-|2\rangle$ EIT, E_{F1} and R_1) will shift from left to right. The two groups of

signals partially overlap when Δ_2=80MHz (Fig. 6(a1)) and Δ_2=40MHz (Fig. 6(a3)), completely overlap when Δ_2=60MHz (Fig. 6(a2)), and finally separate when Δ_2=$-$150MHz (Fig. 6(a4)). When the two groups of signals completely or partially overlap, they will interact with each other. For example, when the two FWM signals completely overlap, the intensity of the total FWM signal is suppressed to its minimum (Fig. 6(a2)), resulting from the strongest mutually dressing effect of $|0\rangle-|1\rangle-|2\rangle$ and $|0\rangle-|1\rangle-|3\rangle$ subsystems.

Then, under the abnormal propagation configuration where E_2 is deflected with α=0.12° (Figs. 6(b1)-6(b4)), the EIT peak of the $|0\rangle-|1\rangle-|2\rangle$ subsystem transforms to an EIA dip. Similar to the case of α=0°, the EIA of $|0\rangle-|1\rangle-|2\rangle$ and EIT of $|0\rangle-|1\rangle-|3\rangle$ partially overlap (Figs. 6(b1) and 6(b3)), completely overlap (Fig. 6(b2)), and finally separate (Fig. 6(b4)). The two groups of characteristic signals still interact with each other. But the interaction behaves differently now. For example, for the FWM in Figs. 6(b1)-6(b3), the sum of E_{F1} and E_{F2} reaches the maximum amplitude when they completely overlap in Fig. 6(b2), which is different from the case in Figs. 6(a1)-6(a3) where the sum of E_{F1} and E_{F2} reaches the minimum amplitude when completely overlapping. This is because the FWM signal E_{F2} get enhancement instead of suppression in the case of α=0.12°. With respect to the fluorescence signal, the two-photon emission peak of R_1 is strengthened in the condition of α=0.12°, corresponding to the $|0\rangle-|1\rangle-|2\rangle$ EIA.

5. Observation of angle modulated suppression-enhancement switch of FWM

In above sections the EIT-EIA switch modulated by angle α has been thoroughly discussed. The angle-modulated suppression-enhancement switch of FWM, on the other hand, only reflects in the variation of signal's amplitude. In this section, we will modulate our spatial geometry so that the switch of FWM could be observed directly. In Fig. 7 and Fig. 8, we adopt the geometry shown in Fig. 1(e), where the external dressing field E_3 instead of self-dressing field E_2 is deflected with the angle β. The corresponding detuning Δ_3 is scanned here.

Figure 7 shows concerning signals with two angle: $\beta = 0$$^\circ$ (normal) for (a1)-(a3), and $\beta = 0.12$$^\circ$ (abnormal) for (b1)-(b3). The behaviors of the probe transmission and the fluorescence signals are similar with above figures, so we mainly focus on the FWM. In Figs. 7(a2) and 7(b2), the curves at discrete Δ_1 points form a double-peak profile (dash line), representing the AT-splitting of FWM signal E_{F1} induced by self dressing effect of E_2 (E_2'). The peak or dip on each baseline, on the other hand, means E_{F1} is enhanced or suppressed by the external dressing field E_3. By manipulating the deflection angle β, we can observe the switch between enhancement and suppression directly. For instance, under the normal case (Fig. 7(a2)), the FWM signal undergoes suppression at the two global peaks (Δ_1=70MHz and Δ_1=115MHz) and the global valley (Δ_1=100MHz), slight enhancement at two edges of the double-peak (Δ_1=40MHz and Δ_1=160MHz), and partial-suppression-partial-enhancement at other points. Now, with β altered to 0.12° (Fig. 7(b2)), the original suppression dips around the left global peak are all replaced by pure enhancement, and around the right global peak the suppression also diminishes obviously. Such suppression-enhancement switch of FWM is in concord with the EIT-EIA switch in Sec. 3 and 4.
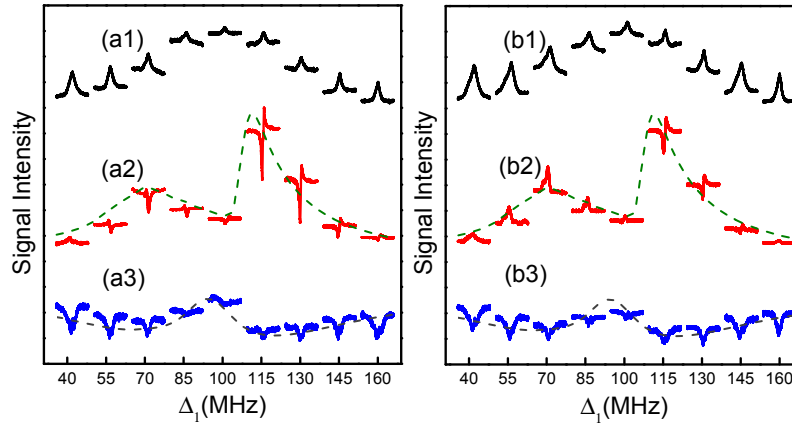
Fig. 7. Measured probe transmission ((a1) and (b1)), FWM signal E_{F1} with enhancement and suppression ((a2) and (b2)), and fluorescence signal ((a3) and (b3)) versus Δ_3 at discrete Δ_1, with fixed $\Delta_2 = -100$MHz and E_3' blocked. The deflection angle β is $\beta = 0°$ for (a1)-(a3), and $\beta = 0.12°$ for (b1)-(b3). The other experimental parameters are $P_1 = 4.5$mW, $P_2 = 12.9$mW, $P_2' = 8.2$mW and $P_3 = 29.0$mW.

Besides, we notice that unlike the strong two-photon fluorescence peak (R_1) in Fig. 4 and Fig. 5, in Figs. 7(a3) and 7(b3) the two-photon fluorescence peak (R_2) is rather weak within each dip of single-photon fluorescence. This difference results from the discrepancy of spontaneous transition probability between the transitions $|2\rangle \rightarrow |1\rangle$ and $|3\rangle \rightarrow |1\rangle$. Theoretical calculation shows that the photons in the excited state $|3\rangle$ ($5D_{3/2}$) are more likely to transit to $5P_{1/2}$ rather than $|1\rangle$ ($5P_{3/2}$), while for the excited state $|2\rangle$ ($5D_{5/2}$) the transition $|2\rangle(5D_{5/2}) \rightarrow |1\rangle(5P_{3/2})$ is dominant [21], which results in R_1 much stronger than R_2.

In Fig. 8, we continuously change β from $-0.04°$ to $0.16°$ with Δ_3 scanned, so that the evolution of the signals versus the deflection angle can be observed more clearly. Figures 8(a) and (b) separately depict the signals at the left and right peaks (corresponding to $\Delta_1=70$MHz and $\Delta_1=115$MHz in Figs. 7(a) and 7(b)) of the FWM double-peak profile. When the angle β changes from negative to positive, the height of EIT for probe transmission signal increases from small to large in the beginning, and then decreases to small again, as shown in Figs. 8(a1) and 8(b1) from top to bottom. For fluorescence signal, we can see the suppression (dip) of it also changes from small to big, then to small with increasing β, as shown in Figs. 8(a3) and 8(b3), corresponding to the variation of probe transmission signal. The enhancement and suppression of the FWM signal E_{F1} are shown in Figs. 8(a2) and 8(b2). At the left peak of the AT splitting double-peak structure (Fig. 8(a2)), the dressing effect on E_{F1} evolutes from pure suppression, to partial-suppression-partial-enhancement, then to pure enhancement with β increasing. Especially, when $\beta = 0°$, the suppression dip gets deepest,
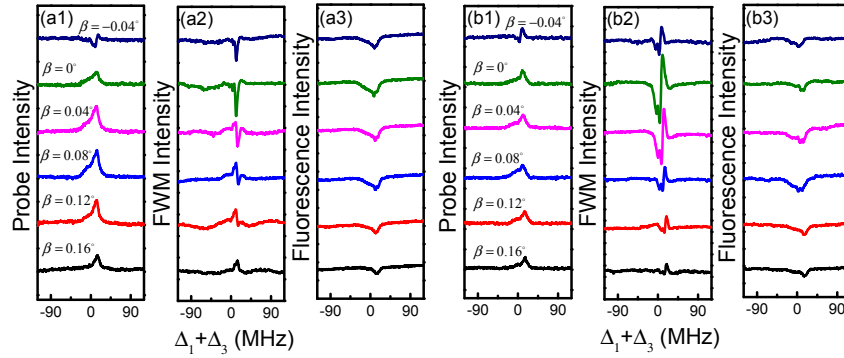
Fig. 8. Measured probe transmission ((a1) and (b1)), the enhancement and suppression of FWM signal E_{F1} ((a2) and (b2)), and fluorescence ((a3) and (b3)) versus Δ_3 with $\beta = -0.04°$, $0°$, $0.04°$, $0.08°$, $0.12°$ and $0.16°$ from top to bottom. (a) and (b) are separately the signals obtained at left peak and right peak of the FWM double-peak profile. The other parameters are $P_1 = 3.6\text{mW}$, $P_2 = 30.6\text{mW}$, $P_2' = 5.4\text{mW}$ and $P_3 = 14.0\text{mW}$.

corresponding to the case in Fig. 7(a2); when $\beta = 0.12°$, E_{F1} undergoes strong enhancement, corresponding to the case in Fig. 7(b2). At the right peak (Fig. 8(b2)), the FWM signal mainly shows the pattern of left-suppression and right-enhancement. Although the switch from suppression to enhancement in Fig. 8(b2) is not as prominent as that in Fig. 8(a2), the tendency could also be seen.

6. Conclusion

We have investigated the four-wave mixing (FWM), fluorescence and the probe transmission simultaneously in the atomic rubidium system. By manipulating the deflection angle of certain coupling beams, the switch between dark state (EIT of probe transmission and suppression of the nonlinear optical processes) and bright state (EIA of probe transmission and enhancement of the nonlinear optical processes) is obtained. We have separately investigated such angle-modulated switch in ladder-type atomic system with singly-dressing effect and Y-type system with doubly-dressing effect. Such angle-modulated switch could have potential applications in optical communication and quantum information processing. Moreover, in the ladder-type system, we have observed and analyzed similarities and discrepancies between the two ground-state hyperfine levels F = 2 and F = 3 of Rb 85.

Acknowledgments